

Deformation and failure mechanism exploration of surrounding rock in huge underground cavern

Zhenhua Tian^{*1,2}, Jian Liu³, Xiaogang Wang^{1,2}, Lipeng Liu^{1,2}, Xiaobo Lv⁴ and Xiaotong Zhang⁴

¹China Institute of Water Resources and Hydropower Research, Beijing 100038, China;

²State Key Laboratory of Simulation and Regulation of Water Cycle in River Basin, Beijing 100038, China;

³Yalong River Hydropower Development Co., Ltd., Chengdu 610051, China;

⁴Luoyun Water Project Management Division of Jiangsu province, Suqian 223800, Jiangsu, China;

(Received March 14, 2019, Revised May 5, 2019, Accepted July 17, 2019)

Abstract. In a super-large underground with “large span and high side wall”, it is buried in mountains with uneven lithology, complicated geostress field and developed geological structure. These surrounding rocks are more susceptible to stability issues during the construction period. This paper takes the left bank of Baihetan hydropower station (span is 34m) as a case study example, wherein the deformation mechanism of surrounding rock appears prominent. Through analysis of geological, geophysical, construction and monitoring data, the deformation characteristics and factors are concluded. The failure mechanism, spatial distribution characteristics, and evolution mechanism are also discussed, where rock mechanics theory, FLAC^{3D} numerical simulation, rock creep theory, and the theory of center point are combined. In general, huge underground cavern stability issues has arisen with respect to huge-scale and adverse geological conditions since settling these issues will have milestone significance based on the evolutionary pattern of the surrounding rock and the correlation analyses, the rational structure of the factors, and the method of nonlinear regression modeling with regard to the construction and development of hydropower engineering projects among the worldwide.

Keywords: hydropower station, underground engineering, surrounding rock deformation, multi-point displacement, monitoring model

1. Introduction

1.1 Research background

The current situation regarding environment and the energy is growing serious; China, a large and responsible country, is engaged in energy structure optimization, with ecology as a priority, to develop clean energy scientifically. Especially, the Jinsha River, Yalong River, Dadu River and Lancang River have been taken as representatives to vigorously develop clean hydropower energy in alpine valleys in southwest China. Some representative projects have been built, such as Xiangjiaba, Xiluodu, Nuozhadu, Xiaowan, Jinping I, Dagangshan and Monkey Rock. And, large hydropower stations such as Baihetan, Wudongde and Yangfanggou are under construction. The scale and difficulty of design and construction of these mega-projects are unprecedented. According to local conditions, the deep underground cavern group is a kind of water diversion power generation solution widely used in the world-class giant power stations in the southwest region. Tab.1 shows the large underground powerhouse structures allocated by the representative projects of the four major hydropower bases.

A high geostress field and a strong new activity are caused because of Indian Ocean plate squeezing the Eurasian plate. Extremely complex geological conditions of deep mountains and valleys are formed in southwest China as the product of historical geological tectonic movement (extrusion, cutting, rising, etc.) (Yang *et al.* 2017, Zhang *et al.* 2012, Wu *et al.* 2016, Wei *et al.* 2019). Large underground caverns with different excavation volume, different section forms and matching functions are arranged according to the situation restricted by factors such as terrain conditions, functional requirements and overall layout of hubs.

There are the characteristics of “large span and high side wall” for most of the underground plant structures in the deeply buried mountains with uneven lithology, complicated geostress field and developed geological structure. The surrounding rocks tend to deform slowly towards the radial direction of the caverns after the excavation of large underground caverns. Nowadays, the NATM (New Austrian Tunneling Method) is widely used in underground engineering home and abroad. The deformation of surrounding rock can be effectively and timely controlled by the principle of shotcrete-anchor support by the capacity of surrounding rock. The stability of surrounding rock of large caverns becomes a major and prominent design and construction challenge for hydropower engineering construction while deep-buried underground caverns in southwest China are located in high mountain valleys with strong tectonic movement and complicated geological conditions.

*Corresponding author, Ph.D. Student
E-mail: tianzhenhua2019@outlook.com;
tianzhenhua_126@126.com

Table1 Statistics of underground powerhouses

Name	Size (Span×height×length/m)	Vertical depth/m	Stress /MPa	Watershed	Status
Jinping I	28.9(25.6)×68.8×277.0	160~420	21.7~35.7	Yalong River	Built
Jinping II	28.3(25.8)×72.2×352.4	231~327	10.1~22.9	Yalong River	Built
Xiluodu	31.9(28.4) ×75.1 ×307.2	340~480	16~18	Jinshajiang	Built
Houziyan	29.2(25.8)×68.7×219.5	400~660	21.5~36.4	Dadu River	Built
Dagangshan	30.8(27.3)×74.6×226.6	390~520	11.4~19.3	Dadu River	Built
Guandi	31.1(29.0)×78.0×243.4	154~427	20.0~35.7	Yalong River	Built
Xiaowan	30.6(25.0)×79.4 ×298.4	380~480	16.4~26.7	Lijiang	Built
Baihetan	34.0(31.0)×88.7×438.0	260~330	19.0~23.0	Jinshajiang	Under construction
Wudongde	32.5(30.5)×89.8×333.0	220~380	7.0~13.5	Jinshajiang	Under construction
Ertan	30.7(25.5)×65.38×280.3	250~350	17.2~38.4	Yalong River	Built
Xiangjiaba	33.0 (31.0)×85.5×245.0	105~225	8.2~12.2	Jinshajiang	Built
Nuozhadu	31.0(29.0)×77.8×418.0	180~220	6.5~10.9	Lijiang	Built
Shuangjiangkou	28.3(25.3)×67.3×214.7	321~498	16.0~37.0	Dadu River	Under construction
Yangfanggou	30.0(27.0)×75.6×228.5	200~330	12.6~13.0	Yalong River	Under construction
Changheba	30.8(27.3)×73.4×228.8	285~480	16.0~32.0	Dadu River	Under construction



Fig. 1 Locations of Baihetan hydropower station

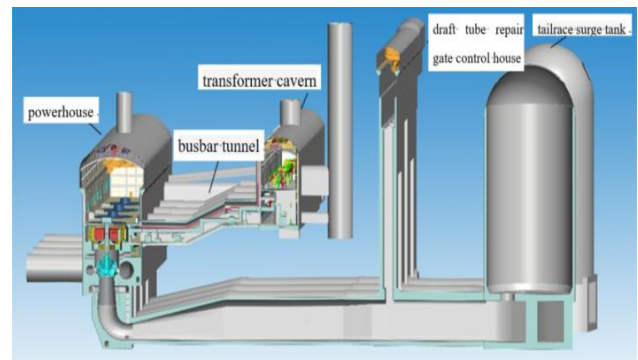


Fig. 2 Cross-section of the four main caverns of underground powerhouse of Baihetan hydropower station

According to the statistics of the main underground caverns before 2006 home and abroad, the large underground caverns with span over 25 m and side wall height over 50 m are called “large-span, high side wall” (Ju *et al.* 2005). In recent years, a series of giant underground projects in southwest China have exceeded 30 m in span and 70 m in height, even more than 80m, which is called “super-large underground caverns”. This paper mainly studies the left bank underground powerhouse of Baihetan Hydropower Station, which is one of them.

As mentioned above, the stability of surrounding rock is always the focus for the scientific researchers and engineers. It is very important to analyze the safety information hiding in the monitoring data of underground engineering and establish the relationship between the monitoring data and the deformation and failure of surrounding rock. It is also very significant to clarify the mechanism of deformation and failure of surrounding rock and reveal its relationship with initial stress field, geological structure, construction progress and supporting structure load. It will more effectively feedback construction design and provide reference for similar projects.

It is taken as the research object in this paper for the underground powerhouse on the left bank of Baihetan, the largest span of cave in China. The achievements and experiences of similar engineering literature are drawn widely. Above analyses are through the means of rock mechanics theory, support design theory, numerical simulation and so on, which is combined with geology, geophysical exploration, monitoring and construction data to qualitatively grasp the distribution and failure law and load response characteristics of supporting structure, etc.

A monitoring model of surrounding rock deformation is explored and established by quantitative analysis of surrounding rock deformation laws with reasonable tectonic factors and above contents.

1.2 Project background

Baihetan hydropower station is located at the junction of Sichuan and Yunnan in the lower reaches of Jinsha river (Chen *et al.* 2018, Chen *et al.* 2016b), with a total reservoir capacity of 20.627 billion m³, a regulating reservoir of

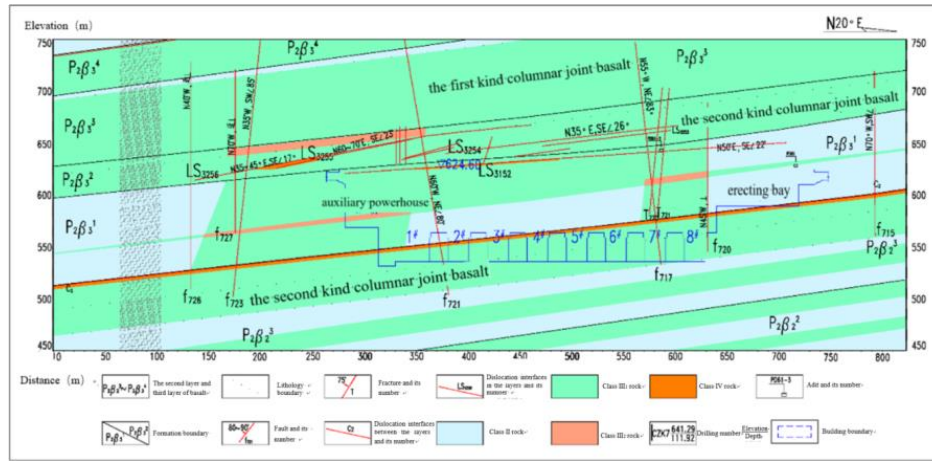


Fig. 3 Engineering geological profile of the underground powerhouse on the left bank

10.436 billion m³, and a flood control reservoir of 7.50 billion m³. After completion, the total installed capacity of the power station will be 16000MW, and 8 hydro-generators of 1000MW will be installed in the underground plants on the left and right bank.

The left and right banks of the diversion power generation system are basically symmetrical, and the head development plan is adopted for the underground powerhouse. The water conveyance system is made up of intake, pressure pipeline, main and auxiliary powerhouse tunnel, main transformer room, tailrace surge chamber and tailrace pipe overhaul gate room, tailrace tunnel overhaul gate room, tailrace tunnel overhaul gate room, tailrace outlet and other buildings. The layout of diversion and tailrace buildings are arranged in the form of single machine with single tunnel and two machines with one tunnel. Three tailrace tunnels on the left bank are combined with diversion tunnels, and two tailrace tunnels on the right bank are combined with diversion tunnels. The main and auxiliary powerhouse caves, main transformer caves, tailrace overhaul gate rooms and tailrace surge chambers are arranged in parallel. The layout pattern of underground powerhouse caverns on the left bank is shown in Fig. 1 (Yang *et al.* 2015a, Chen *et al.* 2016a, Arefian *et al.* 2016). The main and auxiliary powerhouse tunnels are arranged according to the “I” font, and the auxiliary powerhouse, auxiliary installation site, unit section, installation site and air conditioning room are arranged in turn from south to north. The main and auxiliary powerhouse caves are 438m in length, 88.7m in height, 31.0m in width below rock beam and 34.0m in width above rock beam. Roof arch is at an elevation of EL.624.6m. Unit installation is at an elevation of EL.570.0m. Draft tube floor is at an elevation of EL.535.9m.

1.3 Geological conditions

The vertical burial depth of the underground powerhouse of the left bank is about 260~330m. Fig. 3 shows the engineering geological section of the underground powerhouse on the left bank. The stratum is monoclinic structure. The overall occurrence is N40°~45°E,

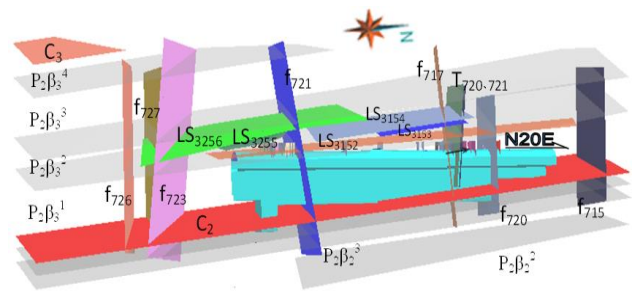


Fig. 4 Spatial distribution of geological structural plane for the underground powerhouse on the left bank

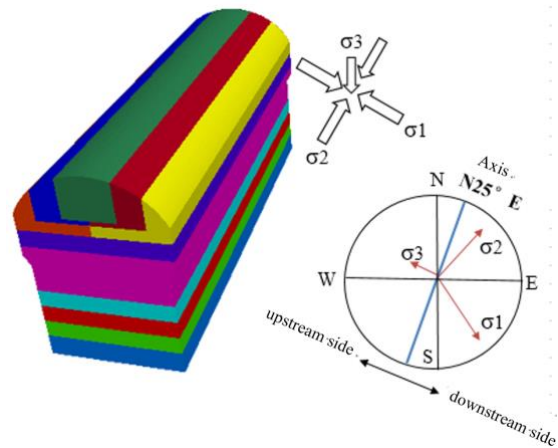


Fig. 5 Diagram of relation between initial ground stress and cavern azimuth of underground powerhouse on left bank

SE∠15°~20° and the strike is about 20°~25° intersecting with the axis of the factory. The lithology is mainly P₂β₃¹ layers of plagioclase basalt, almond basalt, breccia lava and cryptocrystalline basalt. The main type is type III₁, and the local type is type II. The C₂ outcropping area of interlayer staggered zone is type IV.

Fig. 4 shows the spatial distribution of the main geological structural planes in the plant area. Three small faults (f₇₁₇, f₇₂₀, f₇₂₁) are mainly developed in the main and auxiliary powerhouse caves, which are rock debris-type

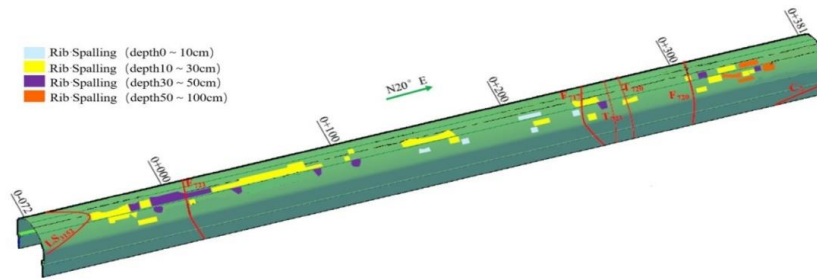


Fig. 6 Spatial distribution of band damage location of main workshop



Fig. 7 Arch surrounding rock of powerhouse

steep dip structural planes, and large cracks (T_{720} , T_{721}) are steep dip rigid structural planes. The interlayer staggered zone C_2 obliquely penetrates the middle and lower part of the side wall of the factory building and develops along the middle part of the $P_2\beta_2^4$ layer tuff with a thickness of 10~30cm and mudstone-intercalated debris type, which is easy to soften in case of water; the interlayer staggered zone LS_{3152} obliquely cuts the southern top of the factory building with a bandwidth of 1-2cm, with breccia structural rock in the zone, and the same group of gently inclined fissures with a bandwidth of 1-2cm, which is a hidden fissure. LS_{3152} and its same group of cracks in the gently inclined layer extend about 150m from the south end of the factory building to the North intermittently. This area is the most obvious section affected by the excavation of the arch ring deformation response and damage phenomenon. The measured maximum cumulative deformation of the crown, the shoulder and the foot of the arch are all distributed in this range. The initial ground stress is determined according to the measured ground stress. The calculation uses the mean value of the ground stress measurement to simulate.

In-situ stress is the mainly tectonic stress, the first and second principal stresses are basically horizontal, and the third principal stress is approximately vertical. The direction of the first principal stress is generally between $N30^\circ\sim 50^\circ W$, the dip angle is $5^\circ\sim 13^\circ$, the magnitude is about 19~23MPa, the second principal stress is about 13~16MPa, and the third principal stress is nearly vertical, the magnitude is equivalent to the self-weight stress of the overlying rock mass, generally between 8.2~12.2MPa. As shown in Fig. 5, the relationship between the in-situ stress in the factory area and the orientation of the cavern is illustrated.

The average saturated compressive strength R_b of underground powerhouse rocks is 74~112MPa, and the rock Strength-Stress ratio (R_b/σ_1) is 3.22~5.89. There is a local stress concentration phenomenon, and the maximum stress

is to more than 30MPa, which generally belongs to high in-situ stress area. The initial first principal stress intersects with the axis direction of the tunnel at a large angle of 50~70, which is not conducive to stability.

2 Deformation and failure characteristics

Excavation in arch area on the top of large underground powerhouse will result in the radial unloading of surrounding rock along the section of the tunnel, and the tangential stress around the tunnel will increase accordingly. Because of the plastic zone and surrounding rock loosening zone in the process of stress deflection and the control of geological structure plane, the crown arch often accompanies the failure of surrounding rock such as slope, block collapse and even rock burst. According to the different decisive factors controlling the failure of the surrounding rock, the failure of the surrounding rock of the underground powerhouse can be divided into three types: stress controlled failure, structure plane controlled failure and stress-structure plane combined controlled failure.

2.1 Stress-controlled failure

The failure of “stress-controlled” surrounding rock is mainly affected by the high in-situ stress level, which mainly includes rock burst, sheet-wall, fracture and so on. The main stress-controlled failure phenomena in the surrounding rock of the arch ring of the ground works on the left bank of Baihetan are the flake and rupture failure. The slope mainly occurs near the excavation contour and belongs to the shallow surface damage of surrounding rock.

As shown in Fig. 6, during the expansion of the middle pilot tunnel and I sequence, the surrounding rock of the top arch and the upper side arch shoulder forms pits due to the destruction of the flange. The pits generally form a platform

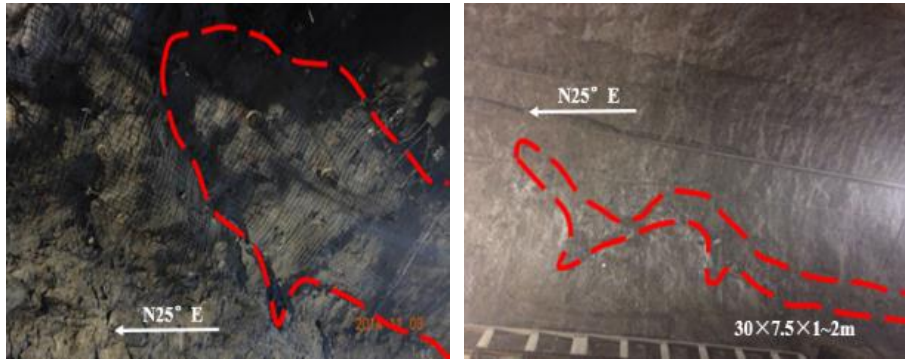


Fig. 8 The collapse of powerhouse's roof arch along the gently inclined angle layer in the LS₃₁₅₂



(a) Upstream arch shoulder rock drum (b) Poor upstream molding (c) The rib arch of upstream side arch is bent
Fig. 9 Surrounding rock failure on the upstream side of the powerhouse

sill in the vertical direction of the axis of the powerhouse. The surrounding rock mass of the platform sill is fractured and destroyed under the influence of high stress when it has been supported (or partially supported), and the fracture surface is nearly parallel to the empty surface of the excavation. The spalling depth of the section affected by LS₃₁₅₂ is generally 10~30cm and 50 cm locally, as shown in Fig. 7.

Due to the constraints of geological conditions and overall hub layout, the axis orientation of the underground powerhouse on the left bank of Baihetan has adopted the N20°E scheme through comprehensive comparison. Under this condition, the direction of the first principal stress intersects the hole axis at a large angle (50°~70°), therefore, the consequence of excavation is that the shear stress concentration will occur in the hole circumference. Liu (Liu *et al.* 2006, Yu *et al.* 2015) and some other professors hold the idea that this is because of the “Source power” which comes up with the damage of rib spalling. In addition, from the perspective of spatial distribution, the rib spalling of weak geological structures such as the fault zone between the factory buildings are less damaged, and the rib spalling are developed in the complete rock mass with the main unstructured surface or the complete rock mass with the hard structural surface.

2.2 Failure type of structural surface control

The main decisive factor of the surrounding rock failure of which the type is called “structural surface control” is the influence of the cutting action of the geological structure surface, resulting the existence of unstable blocks or semi-positioned block boundaries in the surrounding rock. The

exposed part LS₃₁₅₂, where the rock mass is mainly broken of the gently dip angled fault zone in the arch zone of the left bank is mainly the structural fault of “structural surface control type”, and the form of which is the collapse and falling of the structural plane along the gently inclined angle: When the distance between the fault zone and the empty surface is relatively close, it is easy to form a large range of unstable rock mass to cause collapse. The combination of the faulty belt and the steep dip angle crack constitutes a small range of semi-locating block boundary. The combination of locally developed slow dip angle crack and steep dip crack can also produce a smaller range of slumps and drops.

As shown in Fig. 8, the exposed area LS₃₁₅₂ in the layer collapses from the south end wall to the K0 30 pile shoulder to the top arch position of the building, and the collapsed area is strip-shaped. The extension ranges is over 30m, and the widest part is about 7.5m. The depth of the collapse is 0.2~0.5m at the beginning excavation, and the excavation of the III layer is increased to 1~2m.

In addition, the left bank of underground powerhouse has a partial drop during the excavation process, which is mainly affected by the NW-directed steep dip cracks. The scale is small and the damage depth is generally less than 0.3m.

2.3 Stress-Structural surface composite controlled failure

The “stress-structural surface composite controlled type” failure shows that the surrounding rock is affected by the geological structure surface cutting and the unfavorable stress state at the same time. And, the influence degree of

Table 2 Physical and mechanical parameters of surrounding rock

Quality	Bulk modulus /GPa	Shear modulus /GPa	f	c /MPa	Tensile strength /MPa
Basalt II	16.60	12.50	1.48	2.92	3.50
Basalt III ₁	13.58	8.14	1.38	2.56	2.80

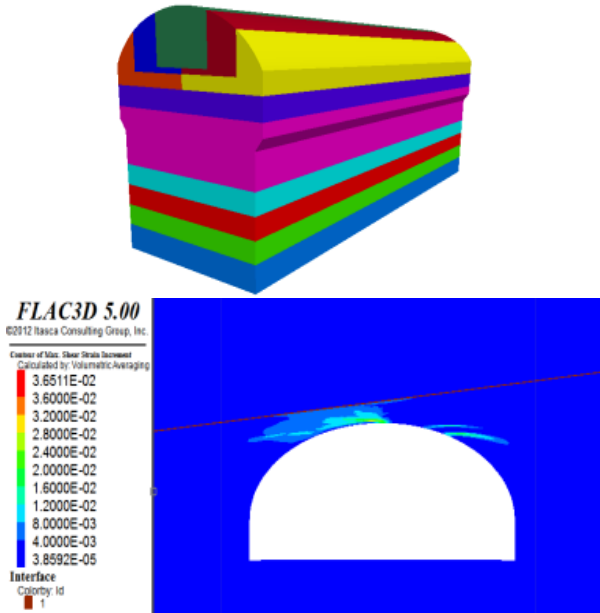


Fig. 10 Shear strain concentration zone of the excavation profile of the main building and the upstream side arch

both is equally important and indispensable. The underground powerhouse of Baihetan left bank has a world-class rare span of 34m. The section span is too large to be excavated at one time. Therefore, the scheme of sequential expansion and excavation is adopted for the surrounding rock of the arch circle, which repeatedly adjusts the surrounding rock stress of the arch circle. There are obvious “bending and breaking” and “bulging out” damage phenomena at the fault zone in the layer at the upstream side of the tunnel section, and the upstream side arch excavation is poorly formed, as shown in Fig. 9. Due to the surrounding rock deformation in this area affected by factors of special geostress, geological structure surface and excavation unloading, etc, it is classified as composite controlled damage.

3. Deformation and failure mechanism of surrounding rock

3.1 “Source force” effect of initial stress field

The original rock stress of the cavern structure is the foundation load of the surrounding rock which is not disturbed by the construction in the three-way confining pressure state. And, it is also an important input factor for the stability analysis of underground engineering. The

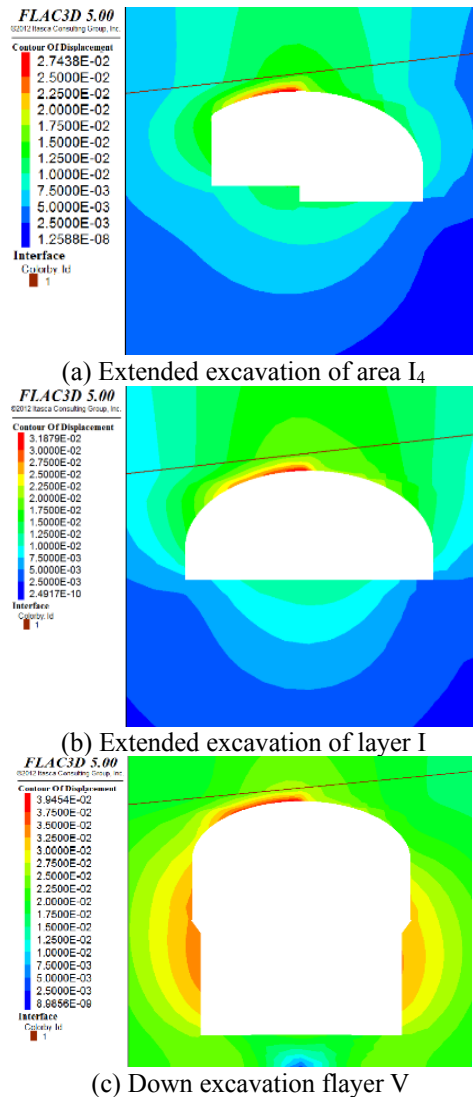


Fig. 11 Evolution process of arch circle deformation field

experience of large underground caverns in the southwestern region indicates that the initial stress field is closely related to the excavation unloading relaxation depth, the surrounding rock failure pattern, the crack propagation of the concrete spray layer and the load response of the supporting structure unit etc (Zhang *et al.* 2017b; Li *et al.* 2009, Yan *et al.* 2008, Zhang *et al.* 2017a). To make the underground powerhouse on the left bank of Baihetan convenient for the overall layout of the hub, and taking into account factors such as avoiding the exposure of the main geological structure to the high stress parts of the cavern, the axis of the comprehensive comparison is arranged at a large angle with the initial first principal stress. From the perspective of initial stress alone, this is a factor that is unfavorable for the stability of surrounding rock (Li *et al.* 2003, Qi *et al.* 2000). Meng and others believe that a good correspondence is with the initial first principal stress for the developmental part of the surrounding rock mass of the top arch (Meng *et al.* 2016) while Liu Guofeng classifies it as the “source force” of the surrounding rock mass destruction (Liu *et al.* 2016, Zhang *et al.* 2018, Yang *et al.* 2015b).

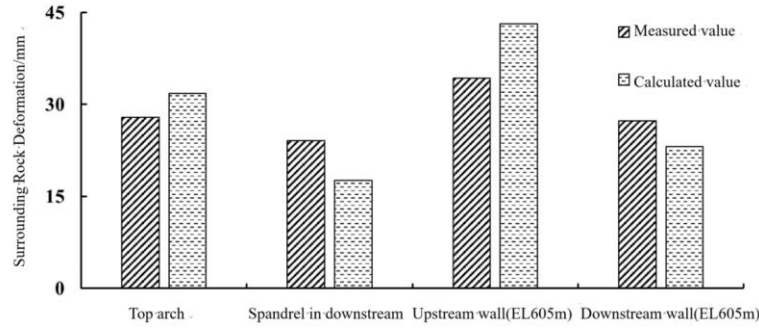


Fig. 12 Comparison of measured and calculated values of surrounding rock deformation of wall of section K0-12 (after layer V is dug)

According to the actual surrounding rock deformation and failure phenomenon, the FLAC^{3D} software is used to simulate the deformation of surrounding rock of the surrounding rock arch of the tunnel. The calculation process considers the influence of sequence excavation, concrete spray layer and anchor follow-up support. Mohr-Coulomb model is used. The constitutive structure of the concrete spray layer and the surrounding rock of the same group of fractured zones are separately elastic and ubiquitous. And, the joint production is consistent with the LS₃₁₅₂. The strength parameter c of the displacement zone is 90 kPa, f is taken as 0.50, and the main parameters of the surrounding rock are listed in Table 2.

The calculation results show that the tangential stress of the arch ring is continuously adjusted due to the sequential excavation. The deformation of the surrounding rock on the downstream side arch is fully released for the area I₂. At this time, due to the unexpanded excavation of the areas I₁ and I₃, the arch effect stress is transmitted, and the surrounding rock of the same group of cracks in the lower side of the upstream side LS₃₁₅₂ is cut with shear stress, producing large shear strain. After the areas I₁ and I₃ are completely excavated, the deformation of the upstream side arch shoulder is also released, and the deformation amount is larger than the downstream side arch shoulder. Fig. 10 shows the concentration zone of shear stress of the upstream side arch after the completion of the middle guide tunnel and the layer I excavation.

The depth of the plastic zone from the top arch to the upstream side arch is 4~9m. The contribution of the middle tunnel and the layer I to the deformation of the surrounding rock of the arch is about 70%~80% (after the layer V₁ is dug), and the evolution of surrounding rock deformation field is shown in Fig. 11, which shows the comparison between measured values and numerical calculations of typical section surrounding rock deformation.

According to the elastoplastic theory, the rock mechanics analysis is carried out to estimate the tangential stress σ_θ

$$\sigma_\theta = \left(\frac{\sigma_v + \sigma_h}{2} \right) \left(1 + \frac{r_0^2}{r^2} \right) - \left(\frac{\sigma_h - \sigma_v}{2} \right) \left(1 + \frac{3r_0^4}{r^2} \right) \cos 2\theta \quad (1)$$

$$\begin{aligned} \sigma_v &= \sigma_3 \\ \sigma_h &= \sigma_1 \sin \alpha + \sigma_2 \cos \alpha \end{aligned} \quad (2)$$

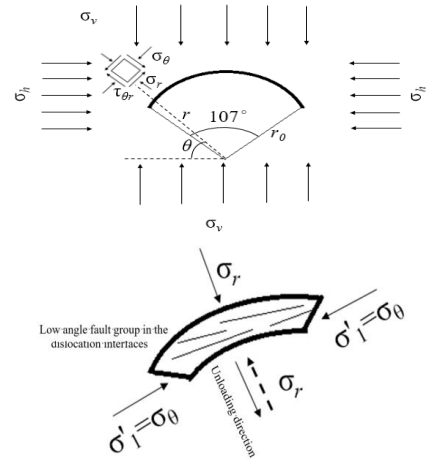


Fig. 13 Calculation diagram of stress redistribution of surrounding rock of arch circle

where r_0 is the radius of the arch circle, m ; r is the radial distance from the center of the arch circle to the arch shoulder of the surrounding rock mass, m ; θ is the polar coordinate angle calculated from the horizontal axis; α is the angle between σ_1 and the axis of the hole, taking 70° . $\sigma_1=23\text{MPa}$, $\sigma_2=16\text{MPa}$, $\sigma_3=12\text{MPa}$, $\theta=45^\circ$.

It is calculated that the tangential stress σ_θ of the upstream side shoulder is about 42.5 MPa.

The rock deformation of the upstream side arch shoulder can be composed of two parts. One is the radial rebound δ_r caused by the unloading of the confining pressure σ_r , and the other is the deformation δ_θ of the surrounding rock caused by the tangential stress redistribution. δ_r and δ_θ are divided into two parts due to the existence of the same group of cracks in the interlayer fault zone

$$\delta_r = \delta_e + \delta_c \quad (3)$$

$$\delta_\theta = \delta_t + \delta_s \quad (4)$$

δ_e is the elastic-plastic rebound caused by radial unloading, δ_c is the crack unfolding caused by radial unloading, δ_t is the elastic deformation caused by the increase of tangential stress and the δ_s is tangential displacement between the cracks of blocks. The numerical results show that the maximum shear strain of the upstream arch is between $6.2 \times 10^{-3} \sim 12.6 \times 10^{-3}$, which shows that the ultimate strain is between 2.0×10^{-3} and 3.5×10^{-3} . Therefore,

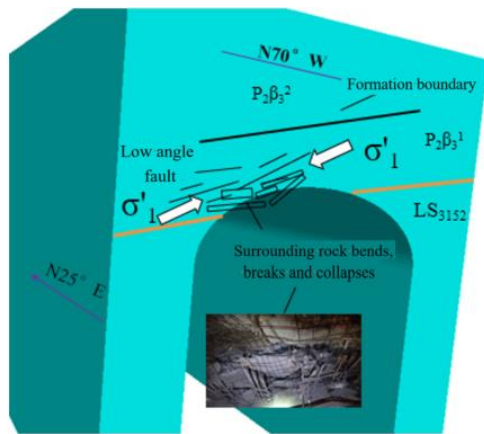


Fig. 14 Mechanical mechanism schematic diagram of rupture failure of surrounding rock of upstream side arch shoulder of typical section

the surrounding rock of the upstream side shallow layer meets the stress-induced splitting stress condition.

According to above analysis, as shown in Fig. 14, the surrounding rock failure of the upstream side arch shoulder is mainly caused by two reasons: There will be fault dislocation happening to the rock of the arch shoulder (waist) and leading to the collapse of exterior as the shear deformation gradually accumulates to a certain amount. The second type is due to the fact that the layered rock mass in this part is crushed or fractured under the influence of shear stress concentration. Therefore, under the combined action of the stress field and the structural surface, the intra-layer fault zone affects the obvious surrounding rock failure during the excavation of the arch ring. Combining with monitoring, geological and numerical simulation, the mechanical mechanism of the circumferential shear deformation of the hole is summarized as follows:

Since the axis of powerhouse intersects with σ_1 at a large angle ($50^\circ\sim 70^\circ$), it is nearly parallel with the strike of the stratosphere, and the excavation causes the secondary tangential stress of the arch ring to increase. The sequence excavation of the layer I cause the surrounding rock to be unloaded in the radial direction. And, the tangential stress is also increased step by step, resulting in stress concentration and then the fault zone in the upstream side of the shoulder layer and its same set of fissures and excavation contours produce shear deformation along the structural surface.

In general, during the excavation of the middle guide hole and the layer I, the deformation of the surrounding rock in the upstream side of the arched shoulder (waist) tends to develop in the direction of the exposed part of excavation, and there is circumferential shear deformation along the circumference of the hole. The monitoring value of the surrounding rock deformation of the point displacement meter shows “negative growth”. The influence of the digging of the layers II and III on the upstream side arch shoulder is weakened, and the deformation of the shallow surrounding rock (within the depth of 3.5m) mainly develops toward the free surface with weak shear stress remained in deep surrounding rock.



Fig. 15 Macroscopic deformation form after completion of C_2 excavation

The excavation of the rock layer below the rock anchor beam produces obvious influence on the upstream side arch shoulder, and the velocity of shallow deformation is still slow at a certain rate (velocity rate of deformation is about 0.05mm/d at 1.5m depth) while the deformation of the surrounding rock tends to converge.

3.2 Control of geological structure

The laminar flow tends to the upstream, and the bedding plane is nearly parallel to σ_1 and σ_2 . The strike intersects with the axis of powerhouse at a small angle, and the excavation is favorable for the bedding stress release. The monitoring results of the inclined hole and dislocation meter indicate that the dislocation belt is insensitive to the external construction disturbance and vibration deformation response, and form a platform with width of 2~5cm within about $1\sim 2d$ after the completion of the excavation as Fig. 15 shows. Thereafter, the velocity rate of deformation of the dislocation belt has been reduced. As described above, due to the soft plasticity of the weak interlayer, the characteristics of deformation are conspicuous.

In the complete or relatively complete rock mass, the deformation is more dispersed along the depth of hole. The time-displacement curve is shown in Fig. 16. The surrounding rock deformation can be divided into two stages: the step-up phase for the excavation response and the progressive convergence phase after the far away excavation section. The deformation of the deep surrounding rock of each hole is “synchronized”, and gradually accumulates from the inside to the outside. This can be attributed to the “stress-controlled” deformation curve. The surrounding rock failure is mainly caused by crack propagation of shallow surface and stress-type failure of rib spalling.

In the area with structural surface development, the deformation along the depth accumulation area of the hole is relatively concentrated, and the time-displacement curve is shown in Fig. 17. There is a large difference in the deformation of the measured points before and after oblique penetration of the staggered zone, which can be attributed to the deformation curve of “structure surface controlled type”. In addition, the deformation aging characteristics are obvious during the excavation interval, and the failure of

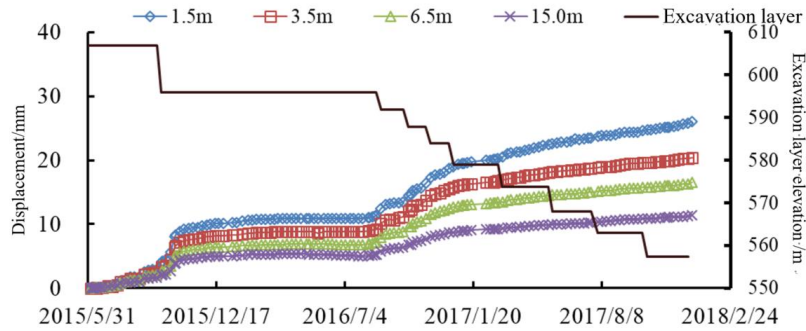


Fig. 16 Time-displacement curve of typical measuring points for “Stress-controlled type” (III₁ nearly complete surrounding rock)

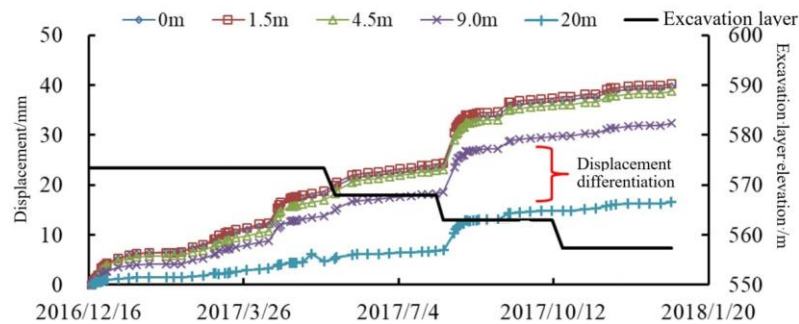


Fig. 17 Time-displacement curve of typical measuring points (influence area of dislocation zone) corresponding to “structural surface controlled type”

the surrounding rock and concrete shotcrete in the affected area is mainly caused by the controlled failure phenomena of structural surface such as dislocation and shear.

3.3 Influence of construction schedule

The analysis object of surrounding rock stability changes with excavation during the process of underground workshop construction. The response mechanism of surrounding rock deformation is very complex. The main factors are: unloading effect caused by stress release, the stress redistribution of surrounding rock caused by stratified excavation, and the changes of engineering properties and boundary conditions of surrounding rocks in different periods, etc.

As shown in Table 3, taking the deformation of surrounding rock at EL.605m elevation of downstream side wall of section K0+229 as an example, and combining with the construction progress analysis, it is concluded:

(1) The deformation response is the most obvious as the distance between elevation excavation and surrounding rock elevation h_e is less than 10m. The deformation rate of shallow surrounding rock at this survey point can reach to 0.15mm/d~0.23mm/d.

(2) The deformation response caused by the excavation of the surrounding rock protective layer belonging to the directly restrained area might not be the largest. The response of the central groove or the excavation of the side wall to the deformation of the section may be more significant (however, all could be attributed to the excavation of the surrounding rock at the same elevation). For example, during the period from June 4, 2015 to

September 16, 2015, the excavation deformation response of the middle groove in section III₁₋₂ and the upstream side protective layer in section III₂₋₂ is more obvious than that of the downstream sidewall protective layer in section III.

(3) During the period of intermittent excavation and shutdown support, the deformation of high sidewall converges quickly, and the deformation rate is not more than 0.01 mm/d.

(4) When the vertical distance between the excavation face and the point h_e is more than 10 m, the deformation rate of the surrounding rock of the high side wall decreases as the excavation elevation decreases.

During the construction, the seismic vibration load also has an effect on the surrounding rock deformation of the high side wall. Yang applied load-unload response ratio theory and numerical analysis method to study that the dislocation zone of Baihetan underground powerhouse is affected by earthquake and the non-linear deformation is strong (Yang *et al.* 2012). Wang believe (Wang *et al.* 2012) that steep dip structural plane is an important factor affecting the stability of surrounding rock of high sidewall under seismic load. In this paper, the effect of seismic load on the structure of underground caverns is illustrated only from a macroscopic point of view.

On the evening of March 12, 2017, a 4.5-magnitude earthquake occurred in Ludian, Zhaotong, which was strongly felt in the Baihetan work area. After the earthquake, the monitoring unit carried out intensive observation. The results showed that the displacement zone and surrounding rock deformation of high sidewall had catastrophic response to seismic loads. The weak links in engineering were exposed by earthquakes.

Table 3 Surrounding rock deformation and construction progress analysis of downstream sidewall, EL.605m in section K0+229

Excavation period	Excavation position	Excavation elevation	Hole depth(m)	Deformation increment(mm)	Deformation rate (mm/d)
2015/5/14~2015/6/3	Layer III K0+268~K0+210 pull slot	607.4	1.5	3.06	0.15
			3.5	2.19	0.11
2015/6/4~2015/6/19	Excavation of layer III downstream sidewall protective layer K0+216~K0+240	605	1.5	2.49	0.17
			3.5	2.10	0.14
2015/7/1~2015/7/30	Extended excavation of upstream side of layer III K0+210~ 0+248 sidewall	600	1.5	5.48	0.19
			3.5	4.09	0.14
2015/8/12~2015/9/16	Excavation of K0+170~K0+230 in the downstream trough III ₁₋₂ area	595	1.5	7.92	0.23
	Excavation of K0+210~K0+235 in the upstream protective layer III ₂₋₂ area		3.5	5.69	0.16
2015/9/23~2015/11/19	Downstream side protective layer III ₂₋₂ area K0+125~K0+307, Upstream side protective layer III ₂₋₃ area slot K0+215~K0+280	595	1.5	11.13	0.2
			3.5	8.22	0.14
2016/1/11~2016/7/12	Shutdown support and rock anchor beam pouring period	591	1.5	1.89	0.01
			3.5	1.45	0.01
2016/8/1~2016/9/26	Excavation of the upstream side of the layer IV of K0+210~K0+270	587	1.5	7.58	0.14
	Excavation of the downstream side of the layer IV of K0+210~K0+250		3.5	6.88	0.12
2016/10/3~2016/10/24	Devilling of K0+195 ~ K0+250 layer V1 , Upstream and downstream excavation of K0+195 ~ K0+255 layer V1	583	1.5	2.29	0.11
			3.5	2.14	0.1
2016/10/31~2016/11/21	Excavation of K0+222 ~ K0+210 layer V2	579	1.5	2.04	0.1
			3.5	1.90	0.09
2016/11/29~2017/1/5	Devilling of K0+190~K0+255 layer VI ₁ Upstream excavation of K0+210~K0+260	579	1.5	2.16	0.05
	Downstream excavation of K0+205~K0+260		3.5	1.98	0.05

Table 4 Statistics of deformation growth of surrounding rocks after earthquakes (typical observation points)

Number of measuring points	Increment of post-earthquake deformation	Position
MZMD7-0+018-1	13.00mm(orifice),13.27mm(3.0m)	crossing openings
Mzc0+267-6	4.28mm(1.5m),3.81mm(3.5m)	around the dislocation belt
Mzzb0+248-1	11.36mm(orifice),10.16mm(3.0m)	steep dip fracture
INzmd3-0+024-1	7.24mm(shear deformation of upper and lower plates)	dislocation belt

The strong deformation response of surrounding rock mainly distributed in the “unloading influence zone” and concentrated around the dislocation belt, the side wall at the development site of steep dip geological structural plane and the crossing openings, shown in Table 4.

3.4 Relevance analysis of surrounding rock deformation and supporting structure load

As an active supporting method, the anchor cable plays a role in restraining the deformation of the surrounding rock. The load change pattern is also related to the surrounding rock deformation. In addition, it is also affected by factors, such as, steel strand stress relaxation, surrounding rock mass and anchor pier creep and construction quality.

The high side walls of the monitoring sections of Baihetan left bank plant are equipped with surrounding rock deformation and anchor cable load measurement points, which provides valuable information for the correlation research of the relevance between above two contents.

Short-term changes: the monitoring results of Baihetan and Dagangshan underground powerhouses show that the prestressing loss of anchor cables after the completion of tension locking lasts about 50-80 days, and the loss rate is between 2% and 7%. In order to eliminate the influence of construction, the typical measurement points with less excavation influence on the early stage of anchor cable locking are selected to analyze the prestress loss law in short-term changes, as shown in Fig. 18. It can be seen that the anchor cable load attenuation law basically conforms to

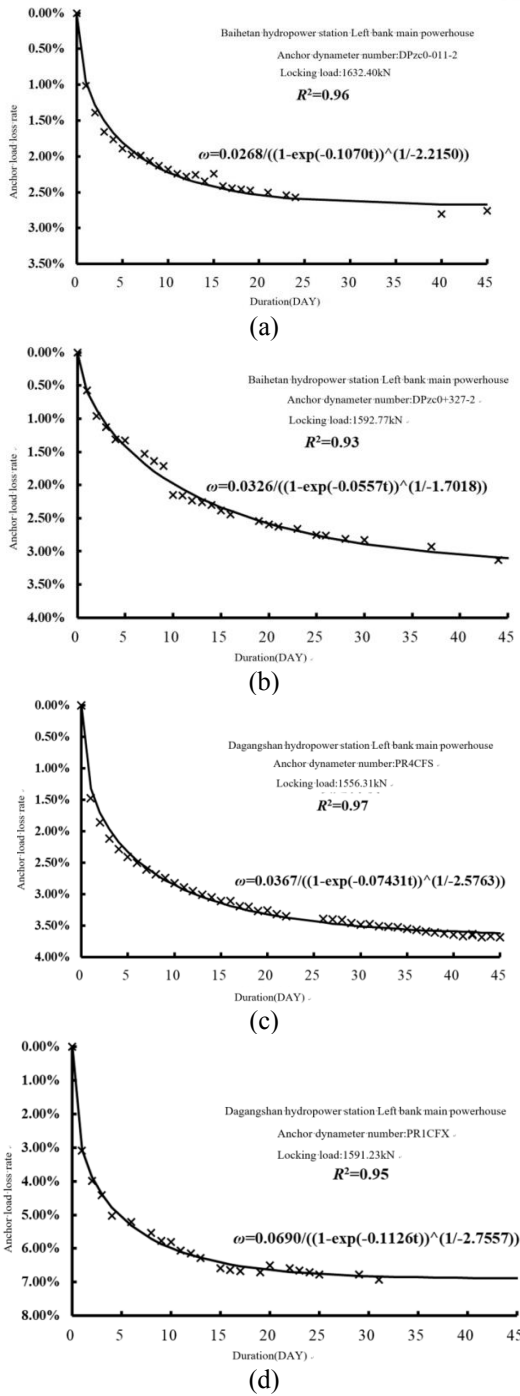


Fig. 18 Load time-loss curve of typical measuring points for anchor cable

the Richards function, and the fitting determination coefficient R^2 is between 0.93 and 0.97. The loss rate ω can be expressed as

$$\omega = c_1 / ((1 - \exp(-c_2 t))^{1/-c_3}) \quad (5)$$

where c_1, c_2 and c_3 are regression coefficients, t is the time after the anchor cable is stretched and locked, and the unit is d .

Long-term changes: After the loss of prestressing force from fast to slow in short-term changes, the load of anchor

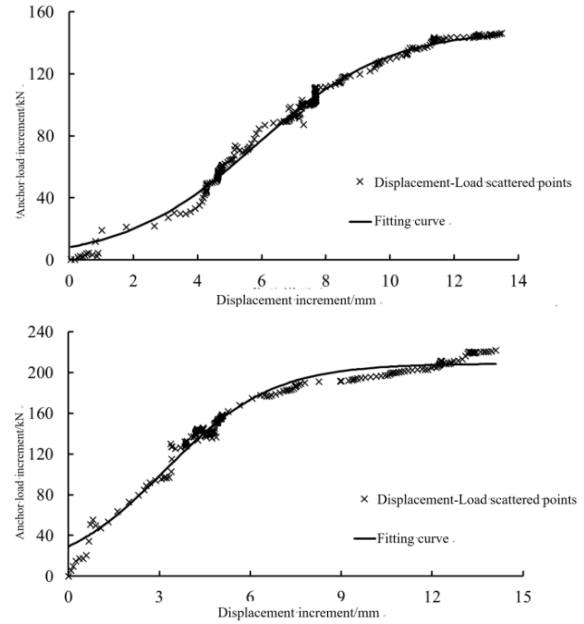


Fig. 19 Correlation analysis of surrounding rock displacement and anchor cable load of typical measuring points

tends to be stable gradually. At this time, as the passive loading, the main factor determining the change of the prestress of the anchor cable is the deformation of the surrounding rock or the unloading of the excavation. After a large number of correlation analysis, the relationship between the displacement increment Δu of the surrounding rock and the load change ΔP can be obtained by using the Logistic regression equation (6), excepting for the relaxation of the steel strand in the initial stage of anchor cable installation or the prestress loss caused by the surrounding rock fissure compaction. The regression equation means:

$$\Delta p = \frac{K}{1 + ae^{-b\Delta u}} \quad (6)$$

where, a, b , and K are regression coefficients, and K is taken as 150kN~350kN. The correlation analysis of typical measuring points is shown in Fig. 19.

4. Monitoring model of surrounding rock deformation

4.1 Model theory and research status

In the design and construction of super large underground caverns, engineers expect to explore the evolution of surrounding rock deformation from existing geophysical, geological, construction, monitoring and other engineering data. According to the existing monitoring data, the method of numerical simulation or mathematical modeling is used to predict, and then feedback to the original design to adjust the construction support plan in time. There are common predictive model methods, such as

regression analysis, gray model, neural network, time series, etc., which often use existing monitoring data as samples or do modeling calculation based on rock mass mechanical parameters (Li *et al.* 2006). These prediction methods have their own advantages and disadvantages. The biggest common problem lies in the improper separation of time and space effects, poor extension, and the inability to adapt to the dynamic conditions of the surrounding rock of the cavern.

The surrounding rock deformation monitoring model of this paper adopts the nonlinear regression method. The basic data of the model comes from the measured data of on-site monitoring. The surrounding rock deformation monitoring instruments of this project mainly include multi-point displacement gauges, anchor dynamometers, anchor stress gauges, etc. These instruments are used to monitor the deformation characteristics of surrounding rock at different depths and the stress of support. The amount of monitoring data is huge. Influenced by the length of the article, this paper only uses the monitoring results data, and does not describe the layout of the engineering monitoring points and the monitoring situation.

Based on the previous research results, combining with the evolution law and correlation analysis of surrounding rock, this chapter reasonably constructs the influencing factors. That is adopted for the method of nonlinear regression modeling to make progress in the establishment of the surrounding rock monitoring model of underground caverns.

It will take on correlation relationship between surrounding rock deformation σ of the cavern and excavation unloading rebound factor δ_e , vibration load factor δ_v , and aging factor (creep) δ_c . Considering the Under certain geological conditions (rock mass, structural surface development, initial stress field, etc.), the surrounding rock deformation. That is, the above influence is taken as an input factor, and the surrounding rock deformation δ is used as an output factor, namely

$$\delta = \zeta(\delta_e, \delta_v, \delta_c) \quad (7)$$

ζ is a nonlinear function, and the difference of local geological conditions is reflected in the solving parameters of model factors under nonlinear correlation between surrounding rock deformation and many factors.

4.2 Model factor construction

The surrounding rock of the underground powerhouse on the left bank of Baihetan Hydropower Station is relatively dry, and there is almost no water seepage. The seepage field has little effect on the deformation of surrounding rock. Similarly, the annual temperature variation of the underground powerhouse of this project is relatively small, and its impact is negligible relative to the excavation unloading rebound factor, shock load factor and aging factor.

The corresponding surrounding rock deformation develops in a "step" shape as the surrounding rock of a large underground cavern is excavated in layers and the elevation of its section decreases in stages. As the distance

between the excavation face and the monitoring deformation points increase, the deformation response gradually weakens, that is, "the distance effect of the excavation face".

It is a problem worth exploring for describing the relationship between excavation unloading and rebound deformation of surrounding rock quantitatively. For the elastoplastic surrounding rock deformation δ_e caused by excavation unloading rebound, according to a large number of Engineering practices, Zhu and others used semi-theoretical and semi-empirical regression method to obtain the prediction formula of elastic-plastic displacement δ_e at key points of high sidewall (Zhu *et al.* 2008)

$$\delta_e = \eta h [a(1000\lambda\gamma H/E)^2 + b(1000\lambda\gamma H/E) + c] \cdot 10^{-3} \quad (8)$$

Therefore, according to formula (8), it can be seen that the elastoplastic displacement of the surrounding rock is proportional to the height of the plant. From another angle, it can be interpreted that there is an approximate linear relationship with the excavation elevation h , so that the unloading rebound deformation component δ_e is

$$\delta_e' = a(h - h_0) \quad (9)$$

In the formula, h_0 is the surrounding rock elevation of the study site, and h is the elevation of the excavation face. However, the unloading factor established by this formula cannot take into account the "distance effect of the excavation face" and therefore has defects. Combined with engineering examples, the quantitative relationship between excavation unloading and surrounding rock deformation of large underground powerhouses is discussed.

Define the unloading response strength Λ (mm/m) as in equation (10)

$$\Lambda = \frac{\Delta\delta}{\Delta h} \quad (10)$$

In the formula, Δh is the height of the excavation layer, and $\Delta\delta$ is the corresponding increment of surrounding rock deformation. Therefore, Λ characterizes the displacement increment of surrounding rock caused by unit excavation elevation.

According to the analysis, the δ_e' in the equation (9) can be multiplied by the attenuation function $\lambda(x)$ to obtain the unloading deformation component function δ_e considering the "distance effect of the excavation face"

$$\delta_e = \delta_e' \cdot \lambda(x) = \frac{a(h - h_0)}{1 + c_1 \cdot (h - h_0) + c_2 \cdot (h - h_0)^2} \quad (11)$$

In the formula, $a = \Lambda_0$, that is, the unloading deformation strength when the excavation face distance is 0. In the actual calculation, it can be obtained by dividing the deformation increment $\Delta\delta_0$ caused by excavation of surrounding rock at the directly constrained monitoring points by the height of excavation layer Δh_0 .

The attenuation function describes the ratio of the unloading strength to the excavation face from the excavation face X . The least squares method is used to fit the formula

$$\lambda(x) = \frac{1}{1 + c_1 \cdot x + c_2 \cdot x^2}$$

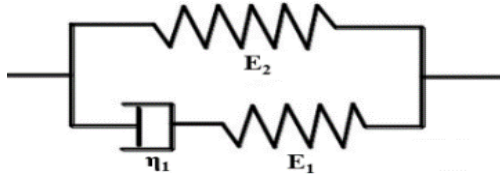


Fig. 20 Composite rheological model of Poyting-Thomson

In the formula, c_1 and c_2 are fitted with attenuation parameters, and the attenuation parameters of different surrounding rock characteristics can be obtained according to the field monitoring data.

According to previous research work and engineering practice, it is shown that surrounding rock deformation caused by blasting construction and seismic vibration load has “mutability” (Yang *et al.* 2012, Wang *et al.* 2012).

Therefore, unit step function $f(x)$ is introduced for simulation, i.e

$$f(x) = \begin{cases} 0 & x < 0 \\ 1 & x \geq 0 \end{cases} \quad (12)$$

There are

$$\delta_v = \sum_i b_i f(\theta - \theta_i) \quad (13)$$

Reorganize θ as the cumulative number of days t divided by 100 in the beginning measurement day of monitoring solstice; reorganize θ_i as for the cumulative number of days t_i divided by 100 from the date of being taken as the i -th vibration step.

As one of the important mechanical properties of rock, the creep of rock is closely related to the long-term stability of engineering. Generally, rock mass creep can be divided into three stages: initial creep, constant creep and accelerated creep (Zhu *et al.* 2010, Wu *et al.* 2003, Sun *et al.* 1999). Since accelerated creep indicates that rock mass is close to failure, it should be avoided in practical engineering. As shown in Fig. 20, the Poyting-thomson rock creep model (hereinafter referred to as PT model) can be used to simulate the aging component. This model can be used to describe the rock mass with elastic hysteresis.

According to the variation trend of deformation over time, the negative exponential function is considered

$$\delta_c = d_1 [1 - \exp(-d_2 (\theta - \theta_0))] \quad (14)$$

In the formula, being reorganized θ_0 is the cumulative number of days (t_0) from the first value of the modeling sequence to the first test day divided by 100.

4.3 Model factor construction

There are non-linear factors in the construction of model factors, and the traditional multiple linear regression method cannot be used to solve the model parameters through regression calculation. Therefore, Marquardt method is used to solve the model parameters. The residual objective function Q is

$$Q(\beta) = \sum_i \{y_i - g(X, \beta)\}^2 \quad (15)$$

where X is the monitoring value vector matrix, β is the parameter solution vector, and g is a nonlinear function of β . The solution process of model parameters is to find β to minimize the objective function Q .

Let $\beta_i = \beta_i^{(0)} + \Delta_i$, $i=1, 2, \dots, m$. Expand $G(X, \beta)$ at the point of $\beta^{(0)}$ into Taylor series, and omit the higher-order terms

$$g(x_k, \beta) = g(x_k, \beta^{(0)}) + \sum \frac{\partial g_{k0}}{\partial b_i} \Delta_i \quad (16)$$

Therefore

$$Q = \sum \left\{ y_k - (g(x_k, \beta^{(0)}) + \sum \frac{\partial g_{k0}}{\partial b_i} \Delta_i) \right\}^2 \quad (17)$$

In order to minimize Q in the sense of least square, the partial derivative with respect is taken to Δ_i and it is set to 0

$$\sum_j k_{ij} \Delta_j = k_{ij} \quad (18)$$

$$k_{ij} = \sum \frac{\partial g_{k0}}{\partial \beta_i} \cdot \frac{\partial g_{k0}}{\partial \beta_j} \quad (19)$$

$$k_{iy} = \sum \frac{\partial g_{k0}}{\partial \beta_i} \cdot (y_k - g_{k0}) \quad (20)$$

The coefficient matrices of the of the equation (17), its right side and Δ_i can be calculated according to equations (16) and (18) as approximation $\beta_i^{(0)}$ and observed value are given. The current β_i is used to replace original approximation $\beta_i^{(0)}$ for next iterative calculation as $|\Delta_i|$ value precision cannot meet the requirements, and until $|\Delta_i|$ meet preset margin of error. Finally the $\beta_i = \beta_i^{(0)} + \Delta_i$ is used to calculate β , a quick model parameters.

4.4 calculation case

Combining with section 3.1 FLAC^{3D} model, three surrounding rock deformation measurement points within the “unloading influence zone” described in section 3.3 were selected for modeling. Fig. 21~Fig. 22 show the time-displacement curve of the typical monitoring model of surrounding rock deformation at measuring points. Tab.5 shows the statistical table of its correlation analysis. It can be seen that there is a good fitting accuracy, and the determination coefficient R^2 of the four selected measuring points, between 0.869 and 0.926 for the “stress-controlled” surrounding rock deformation model (or the surrounding rock deformation that is “stepped” under the influence of fractured section and geological structure plane).

For the wall surrounding rock with good lithology, unloading rebound deformation is the leading factor for the development of surrounding rock to the face of void. The deformation of surrounding rock rapidly converts with the end of stratified excavation, and the aging characteristics

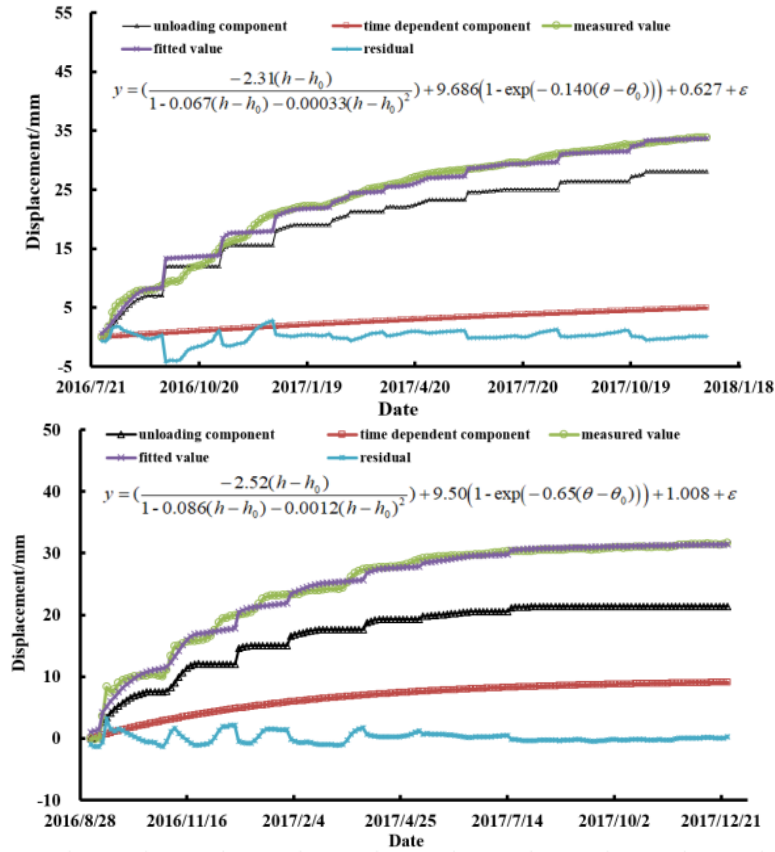


Fig. 21 Time-displacement curves of the upstream wall surrounding rock deformation monitoring model of K0+229 and K0-052 sections

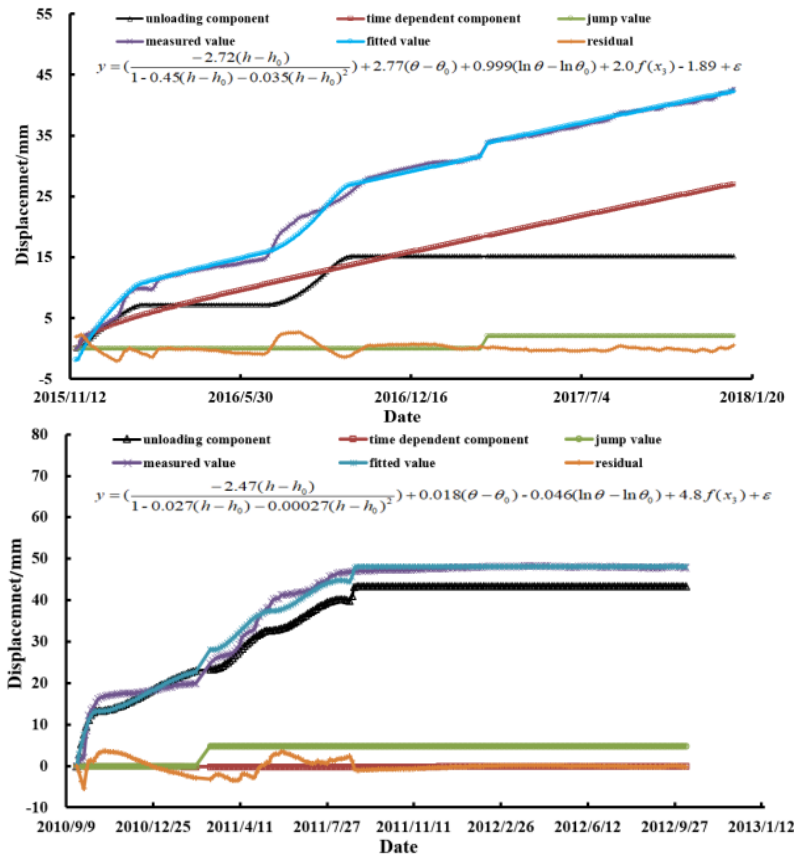


Fig. 22 The time displacement curve of the surrounding rock deformation monitoring model of K0+328 and the upstream side wall of the section of Dagangshan hydropower station (EL.599m)

Table 5 Correlation statistical table of typical monitoring model of surrounding rock deformation

The measuring point section	The location of elevation	R^2	Residual standard S	Unloading rebound deformation component	Aging component	Note
K0+229	The upstream side wall EL.600m	0.882	1.757mm	75%~85%	10%~15%	The core is relatively complete
K0-052	The upstream side wall EL.593m	0.926	1.354mm	65%~70%	20%~25%	The core has broken segments
K0+328	The upstream side wall EL.599m	0.869	1.188mm	30%~40%	50%~55%	Stagger zone development
Dagangshan 4#	The upstream side wall EL.959m	0.911	1.620mm	90%	< 5%	Stress control type

Table 6 The timing table of the modeling and prediction of the typical monitoring model

The measuring point section	The location of elevation	The sequential of the modeling	The sequential of predicting	R^2	Residual standard S
K0-012	The upstream side wall EL.600m	2016/1/21~2017/3/31	2017/4/3~2018/4/11	0.906	0.947mm
K0+077	The downstream side wall EL.600m	2016/9/3~2017/3/29	2017/4/1~2018/4/11	0.867	1.145mm

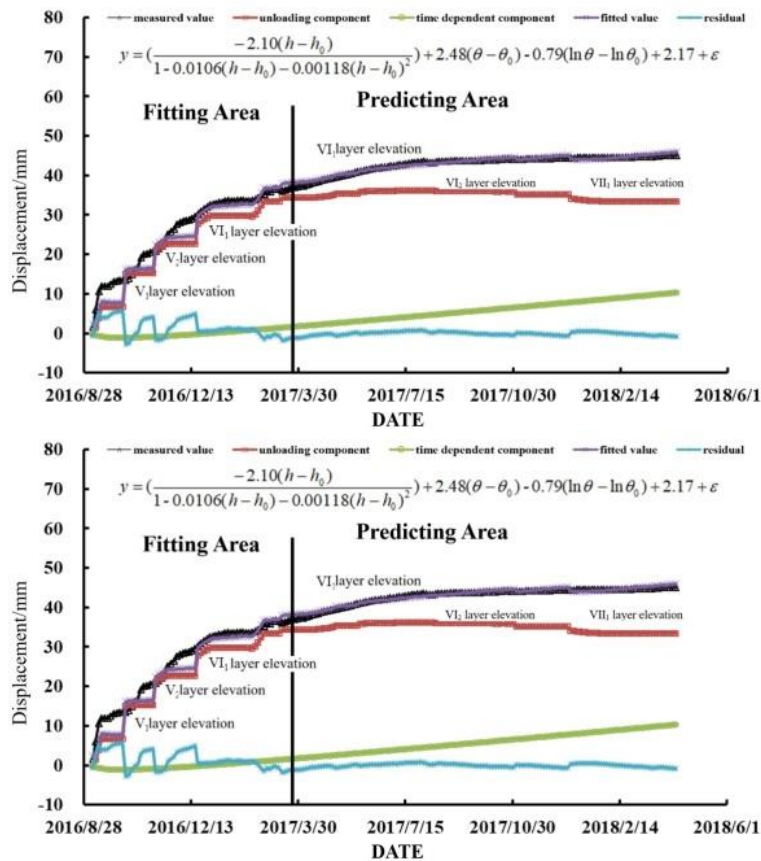


Fig. 23 Time-displacement curves of surrounding rock deformation monitoring model of upstream boundary wall in k0-012 and K0+077 sections

are not obvious. For the part with broken section in the core, there is a difference in deformation along the hole depth, that is, there is a “fracture displacement”, therefore, the proportion of “aging component” is slightly larger, accounting for about 20%~25% of the total deformation. In areas with fault zones, the stress release process is slow due to the flexible plasticity of the weak structural surface. Therefore, the deformation does not converge with the advancing and moving away of the excavation surface. And, the aging characteristics are obvious.

As shown in Fig. 23, the measured deformation monitoring data of typical monitoring points during the excavation from floor IV to floor VI₂ were used for modeling. And, the related variable factors were established based on the data of the VII₁ floor, the subsequent excavation progress and the implementation period. The deformation results after April 1, 2017 were predicted and compared with the actual monitoring results.

This paper gives the proportion of the unloading springback deformation component and aging component of the surrounding rock deformation monitoring model, and gives its surrounding rock characteristics. The unloading springback deformation component is greater than 75%, which indicates that the surrounding rock integrity is better and the support can be reduced; the unloading springback deformation component is less than 70%, indicating that the surrounding rock has a fracture zone. When the aging component is greater than 50%, there is a high possibility that the surrounding rock has a development of the wrong zone, and it is necessary to strengthen support and on-site monitoring. Based on the monitoring model, this paper proposes monitoring indicators to achieve effective monitoring of subsequent deformation of surrounding rock.

5. Conclusions

The main conclusions were presented based on above researches:

(1) The stress state change of the shallow surrounding rock of the high side wall was studied and divided into four stages. It was revealed that there were three types of surrounding rock deformation failures: stress controlled failure, structure plane controlled failure and stress-structure plane combined controlled failure.

(2) The deformation and failure mechanism was studied. The initial geostress, the occurrence of the stratosphere and the nature of the weak interlayer were the prerequisites for the geological structure deformation, which were the “internal factors”. Construction and other external load factors were the “external factors” that induce deformation of the weak interlayer. The “internal factors” determines the “threshold” and type of deformation, and the “external factors” determined the magnitude and size of deformation.

(3) This paper summarized the similar engineering experience, and made an exploratory attempt and research on the establishment of surrounding rock deformation monitoring model by means of FLAC^{3D} numerical simulation and combined rheological model.

(4) This paper also proposed the model of unloading springback, vibration load and aging (creep). The

calculation example was proved that the model had good fitting precision and extension for the development of deformation to the free surface.

Acknowledgments

The research described in this paper was financially supported by the National Natural Science Foundation of China (SN: 51609266, 51879284).

References

- Arefian, A., Noorzad, A., Ghaemian, M. and Hosseini, A. (2016), “Seismic evaluation of cemented material dams -A case study of Tobetsu dam in Japan”, *Earthq. Struct.*, **10**(3), 717-733. <http://dx.doi.org/10.12989/eas.2016.10.3.717>.
- Chen, B., Hu, T., Huang, Z. and Fang, C. (2018), “A Spatio-temporal Clustering and Diagnosis Method of Deformation Monitoring Data in Concrete Arch Dam”, *Struct. Health. Monit.*, **18**(5-6), 1355-1371. <https://doi.org/10.1177/1475921718797949>.
- Chen, Z., Zhao, H. and Lou, M. (2016a), “Seismic performance and optimal design of framed underground structures with lead-rubber bearings”, *Struct. Eng. Mech.*, **58**(2), 259-276. <http://dx.doi.org/10.12989/sem.2016.58.2.259>.
- Chen, S.S., Fu, Z.Z., Wei, K.M. and Han, H.Q. (2016b), “Seismic responses of high concrete face rockfill dams: A case study”, *Water Sci. Eng.*, **9**(3), 195-204. <http://doi.org/10.1016/j.wse.2016.09.002>.
- Ju, N. (2005), “Stability evaluation of surrounding rock mass of underground caverns with large span and high side wall and systematic engineering geology research of supporting scheme”, Ph.D. Dissertation, Chengdu university of technology, Chengdu.
- Liu, G., Feng, T., Jiang, Q., Duan, S., Yao, Z., Pei, S., Duan, X. and Zhou, M. (2016), “Study on characteristics, rules and mechanism of surrounding rock sheet failure in excavation of a large underground workshop in Baihetan”, *Chin. J. Rock Mech. and Eng.*, **35**(5), 865-878. <http://dx.doi.org/10.13722/j.cnki.jrme.2015.0933>.
- Li, L., He, J., Yu, T. and Fan, J. (2003), “Optimization design of vertical axis of underground workshop”, *J. Sichuan Univ.*, **35**(3), 34-37. <http://dx.doi.org/10.3969/j.issn.1009-3087.2003.03.008>.
- Li, Y., Li, X. and Zhang, C. (2006), “The prediction method of surrounding rock displacement based on BP network”, *Chin. J. Rock Mech. Eng.*, **25**(z1), 2969-2973. <http://dx.doi.org/10.3321/j.issn:1000-6915.2006.z1.056>.
- Li, Z., Zhou, Z., Tang, X., Liao, C., Hou, D., Xing, X., Zhang, Z., Liu, Z. and Chen, Q. (2009), “Stability analysis and consideration of underground powerhouse grotto group of Jinping hydropower station”, *Chin. J. Rock Mech. Eng.*, **28**(11), 2167-2175. <http://dx.doi.org/10.3321/j.issn:1000-6915.2009.11.002>.
- Meng, G., Fan, Y., Jiang, Y., He, W., Pan, Y. and Li, Y. (2016), “Study on key rock mechanics problems and engineering countermeasures of giant underground caverns in Baihetan hydropower station”, *Chin. J. Rock Mech. Eng.*, **35**(12), 2549-2560. <http://dx.doi.org/10.3973/j.issn.2096-4498.2016.12.005>.
- Qi, L. and Ma, Q. (2000), “Based on the analysis of geostress field, the selection of long axis of underground cavern and the stability of surrounding rock are discussed”, *Chin. J. Rock Mech. Eng.*, **19**(z1), 1120-1123. <http://dx.doi.org/10.3321/j.issn:1000-6915.2000.z1.065>.
- Sun, J. (1999), *Rheology and Engineering Application of Geotechnical Materials*, China Building Industry Press, Beijing, China.
- Wang, S., Sheng, Q., Zhu, Z. and Xiao, P. (2012), “Study on the mechanism of adverse geological structure collapse of underground caverns under earthquake load”, *Rock Soil Mech.*

- 33(10), 2897-2902. <http://dx.doi.org/10.3321/j.issn:1000-6915.2000.z1.065>.
- Wei, B., Yuan, D., Li, H. and Xu, Z. (2019), "Combination forecast model for concrete dam displacement considering residual correction", *Struct. Health. Monit.*, **18**(1), 232-244. <http://dx.doi.org/10.1177/1475921717748608>.
- Wu, B., Wu, Z., Chen, B., Su, H., Bao, T. and Wang, S. (2016), "Crack status analysis for concrete dam based on measured entropy", *Sci. China Technol. Sc.*, **59**(5), 777-782. <http://dx.doi.org/10.1007/s11431-016-6018-1>.
- Wu, Z. (2003), *The Theory and Application of Safety Monitoring in Hydraulic Structures*, Higher Education Press, Beijing, China.
- Yan, P., Lu, W. and Zhou, C. (2008), "Vibration induced by dynamic unloading of ground stress during blasting excavation in non-uniform stress field", *Chin. J. Rock Mech. and Eng.*, **27**(4), 773-781. <http://dx.doi.org/10.3321/j.issn:1000-6915.2008.04.017>.
- Yang, M., Su, H. and Wen, Z. (2017), "An approach of evaluation and mechanism study on the high and steep rock slope in water conservancy project", *Comput. Concrete*, **19**(5), 527-535. <http://dx.doi.org/10.12989/cac.2017.19.5.527>.
- Yang, M., Su, H. and Yan, X. (2015a), "Computation and Analysis of High Rocky Slope Safety in a Water Conservancy Project", *Discrete Dyn. Nat. Soc.*, **2015**. <http://dx.doi.org/10.1155/2015/197579>.
- Yang, M. and Liu, S. (2015b), "Field tests and finite element modeling of a Prestressed Concrete Pipe pile-composite foundation", *KSCE J. Civil Eng.*, **19**(7), 2067-2074. <http://dx.doi.org/10.1007/s12205-015-0549-z>.
- Yang, J., Sheng, Q. and Zhu, Z. and Leng, X. (2012), "Loading/unloading response ratio study of seismic response on underground rock cavern group", *Rock Soil Mech.*, **33**(7), 2127-2132. <http://dx.doi.org/10.16285/j.rsm.2012.07.014>.
- Yu, S., Zhu, W., Yang, W., Zhang, D.F. and Ma, Q.S. (2015), "Rock bridge fracture model and stability analysis of surrounding rock in underground cavern group", *Struct. Eng. Mech.*, **53**(3), 481-495. <http://dx.doi.org/10.12989/sem.2015.53.3.481>.
- Zhang, Y., Xiao, P., Ding, X., Ou, W., Lu, B., Liao, C. and Dong, Z. (2012), "Study of deformation and failure characteristics for surrounding rocks of underground powerhouse caverns under high geostress condition and countermeasures", *Chin. J. Rock Mech. Eng.*, **31**(2), 228-244. <http://dx.doi.org/10.3969/j.issn.1000-6915.2012.02.002>.
- Zhu, W., Sui B., Li, X. J., Li, S. C. and Wang, W.T. (2008), "A methodology for studying the high wall displacement of large scale underground cavern complexes and its applications", *Tunnel. Underground Space Technol.*, **23**(6), 651-664. <http://dx.doi.org/10.1016/j.tust.2007.12.009>.
- Zhu, H., Yin, J., Dong, J. and Zhang, L. (2010), "Physical modelling of sliding failure of concrete gravity dam under overloading condition", *Geomech. Eng.*, **2**(2), 89-106. <http://dx.doi.org/10.12989/gae.2010.2.2.089>.
- Zhang, Y., Xu, W., Shao, J., Zhao, H. and Wang, W. (2017a), "Experimental investigation of creep behavior of clastic rock in Xiangjiaba Hydropower Project", *Water Sci. Eng.*, **8**(1), 55-62. <http://dx.doi.org/10.1016/j.wse.2015.01.005>.
- Zhang, N. and Evans, T.M. (2018), "Three dimensional discrete element method simulations of interface shear", *Soils Found.*, **58**(4), 941-956. <http://dx.doi.org/10.1061/9780784480137.048>.
- Zhang, N. and Su, H.Z. (2017b), "Application assessments of concrete piezoelectric smart module in civil engineering", *Smart. Struct. Syst.*, **19**(5), 499-512. <http://dx.doi.org/10.12989/sss.2017.19.5.499>.